In situ measurement of light polarization with ellipticity-induced nonlinear magneto-optical rotation

Derek F. Jackson Kimball,[*] Jordan Dudley, Yan Li, and Dilan Patel

Department of Physics, California State University—East Bay, Hayward, California 94542-3084, USA

(Received 3 July 2017; published 12 September 2017)

A precise, accurate, and relatively straightforward *in situ* method to measure and control the ellipticity of light resonantly interacting with an atomic vapor is described. The technique can be used to minimize vector light shifts. The method involves measurement of ellipticity-induced resonances in the magnetic-field dependence of nonlinear magneto-optical rotation of frequency-modulated light. The light propagation direction is orthogonal to the applied magnetic field **B** and the major axis of the light polarization ellipse is along **B**. When the light modulation frequency matches the Larmor frequency, elliptically polarized light produces a precessing atomic spin orientation transverse to **B** via synchronous optical pumping. The precessing spin orientation causes optical rotation oscillating at the Larmor frequency by modulating the atomic vapor's circular birefringence. Based on this technique's precision, *in situ* nature (which avoids systematic errors arising from optical interfaces) and independent control of the most important systematic errors, it is shown that the accuracy of light ellipticity measurements achievable with this technique can exceed that of existing methods by orders of magnitude.

I. INTRODUCTION

Precise control of light polarization is crucial for many atomic physics experiments. Elliptically polarized light causes vector light shifts—ac Stark shifts proportional to an atomic state's magnetic quantum number—that affect atomic energy levels in a manner similar to that of a magnetic field [1–4]. On the one hand, vector light shifts are useful, e.g., for manipulation of ultracold atomic gases [5–8] and for quantum information processing [9], while, on the other hand, vector light shifts cause troublesome systematic effects in atomic clocks [10,11], magnetometers [12–14], and precision tests of fundamental physics [15–17]. There have been a number of recent approaches developed to measure and control vector light shifts: for example, Zhu *et al.* [18] used a variation of the Hanlé effect [19] with Cs atoms trapped in an optical lattice and Wood *et al.* [20] performed differential Ramsey interferometry on a pair of Bose-Einstein condensates. As noted in Refs. [18,20], although there are well-developed techniques for highly sensitive measurements of small polarization *changes* [21,22], these techniques generally do not give absolute measurements of the polarization at similar levels—they are typically limited to accuracies of $\sim 10^{-4}$ rad [21]. Here we present a sensitive, straightforward, *in situ* method to measure light ellipticity applicable to a diverse array of atomic physics experiments.

Our method employs nonlinear magneto-optical rotation (NMOR) resonances that arise when elliptically polarized light propagates through an atomic vapor. Experimental techniques involving NMOR [23] are applied to diverse problems in magnetometry [13,24], quantum and nonlinear optics [23,25–29], and precision measurements [16,30–32]. Our experiment takes advantage of narrow NMOR resonances related to long-lived, ground-state atomic spin polarization moments [33–36], which generically appear in atomic systems with slow relaxation of Zeeman coherences (long T_2)—precisely those systems most significantly affected by vector light shifts. In

our case, the long T_2 times are achieved by using an evacuated vapor cell whose inner surface is covered with an antirelaxation coating that enables atoms to bounce off the cell walls up to a million times while preserving their spin polarization [37]; similar effects should appear in any system with long T_2 times (for example, cold atoms trapped in far-detuned optical lattices [38,39] and nitrogen-vacancy centers in diamonds [40,41]). For the antirelaxation-coated rubidium (Rb) vapor cell used in these experiments, $T_2 \approx 320$ ms and is limited by spin-exchange collisions between Rb atoms [16].

When the light-atom interaction is modulated at frequency Ω_m, NMOR resonances related to different physical effects appear at different magnetic fields. In this work we employ NMOR of frequency-modulated light (FM NMOR) [36], in which a single cw light beam is used for optical pumping and probing of the atomic spin polarization; analogous effects can be achieved in setups using amplitude-modulated light (AM NMOR) [42,43]. Note that superior sensitivity can often be achieved in two-beam arrangements where the pump and probe beam characteristics (power, detuning, etc.) can be separately optimized [44]. In experiments with modulated light, in addition to the zero-field NMOR resonance, resonances appear at magnetic fields where [25]:

$$\Omega_m = \kappa \Omega_L, \tag{1}$$

where Ω_L is the Larmor frequency and κ is an integer associated with the rank of the atomic spin polarization moment (PM) causing the optical rotation. The spatial distribution of angular momentum for the q component of a PM has $|q|$-fold symmetry about the quantization axis, and the maximum possible q is equal to the rank κ. For example, $\kappa = |q| = 1$ corresponds to orientation or a dipole moment (where the spin has a preferred direction or onefold symmetry) and $\kappa = |q| = 2$ corresponds to alignment or a quadrupole moment (where the spin has a preferred axis but no preferred direction, i.e., twofold symmetry). This explains the resonance condition: a PM returns to its initial configuration after rotation of the spins by $2\pi/\kappa$, and so the condition for synchronous optical pumping of a PM of a particular κ is given by Eq. (1). In

─────────
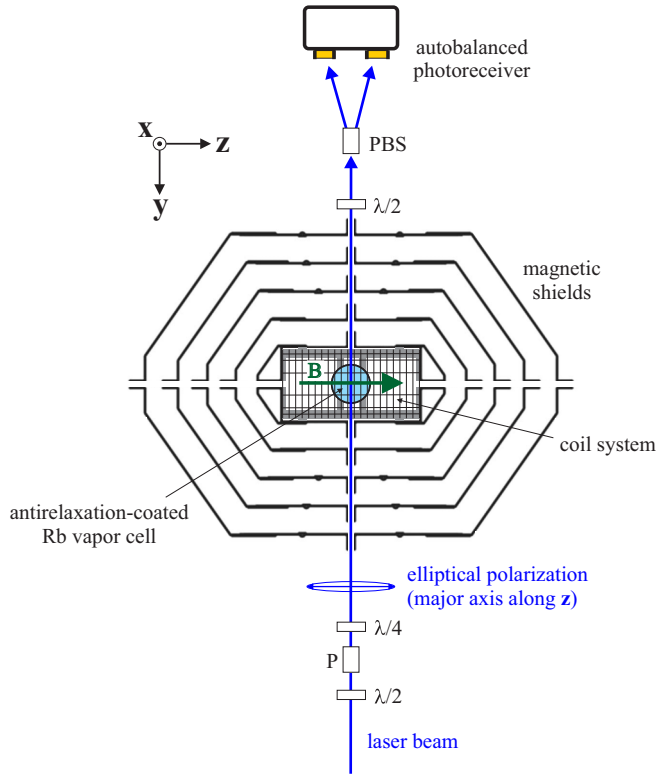[*]derek.jacksonkimball@csueastbay.edu

FIG. 1. Schematic of the experimental setup. P, linear polarizer; PBS, polarizing beam splitter; $\lambda/4$, quarter-wave plate; $\lambda/2$, half-wave plate. Designation of the **x**, **y**, and **z** directions is shown in the upper-left corner. The green arrow at the center of the diagram represents the applied magnetic field **B**. Assorted optics and electronics for laser control, data acquisition, and experiment control are not shown.

turn, the precessing PM modulates the optical properties of the medium at $\kappa\Omega_L$, leading to an observable FM NMOR signal (see detailed discussions in Refs. [13,45]).

In the present work we investigate particular FM NMOR resonances generated by elliptically polarized light. The ellipticity-induced FM NMOR (EI FM NMOR) resonances provide an *in situ* method to directly measure the light ellipticity inside a vapor cell using the atoms themselves as the sensors. When light enters a vapor cell or passes through a window into a vacuum chamber, the polarization of the light is affected by the birefringence of the transparent material making up the cell wall or window. This causes initially linearly polarized light to become elliptically polarized, leading to uncontrolled vector light shifts that can adversely affect the accuracy of magnetometers [46–48] and other precision measurements based on spin precession [16,17]. Note that elliptically polarized light has proven useful for eliminating dead zones in optical magnetometers [49] and for enhancing the amplitude of the zero-field NMOR resonance [47].

II. EXPERIMENTAL SETUP AND PROCEDURE

A simplified diagram depicting the experimental setup and geometry is shown in Fig. 1 (further details concerning the experimental apparatus are given in Refs. [16,50]). An

alkene-coated vapor cell (diameter, 5 cm), containing a natural isotopic mixture of Rb vapor (72% ^{85}Rb, 28% ^{87}Rb), is at the center of a system of coils nested within the innermost layer of a five-layer mu-metal shield [51,52]. The cell temperature was stabilized at 28.4 °C, corresponding to a Rb vapor density $\approx 2 \times 10^{10}$ atoms/cm^3. The coils enable control of all three orthogonal components of the magnetic field and compensation of all first-order gradients. A magnetic field **B** is applied along the z axis, perpendicular to the direction of propagation of the laser beam. Note that this geometry, the so-called Voigt geometry, is different from the Faraday geometry typically used in single-beam NMOR experiments. The major axis of the polarization ellipse of the light is aligned parallel to **B** (along z). The laser light, near-resonant with the Rb D2 transition ($^2S_{1/2} \to {}^2P_{3/2}$), is produced by a tunable external-cavity diode laser (Toptica DL100) and frequency modulated at Ω_m via sinusoidal laser diode current modulation. The laser beam diameter is ≈ 2 mm. Prior to entering the vapor cell, the probe beam passes through a $\lambda/2$ plate, a linear polarizer, and a $\lambda/4$ plate; these optical elements can be adjusted to control the input light's intensity and polarization, which are measured using a ThorLABs PAX720IR1-T polarimeter system. The polarimeter (not shown in Fig. 1) is inserted into and removed from the beam path as necessary. After exiting the antirelaxation-coated vapor cell, the beam is analyzed with a polarimeter consisting of a Wollaston prism polarizing beam splitter whose output rays are detected with an autobalanced photoreceiver (New Focus Nirvana 2007). The signal from the autobalanced photoreceiver is sent to the input of a digital lock-in amplifier (Signal Recovery model 7265) and demodulated at the first harmonic of Ω_m.

The light ellipticity ε is defined in terms of the normalized Stokes parameter S_3 (see, for example, Ref. [53] for a detailed discussion):

$$\varepsilon = \tfrac{1}{2} \arcsin S_3. \tag{2}$$

The optical rotation angle φ is defined in terms of the normalized Stokes parameters S_1 and S_2 [53]:

$$\varphi = \frac{1}{2} \arctan\left(\frac{S_2}{S_1}\right). \tag{3}$$

For our experimental geometry

$$S_1 = (I_z - I_x)/I_{\text{tot}}, \tag{4}$$

$$S_2 = (I_{+\pi/4} - I_{-\pi/4})/I_{\text{tot}}, \tag{5}$$

$$S_3 = (I_+ - I_-)/I_{\text{tot}}, \tag{6}$$

where I_z and I_x are the light intensities along the z and x axes, $I_{+\pi/4}$ and $I_{-\pi/4}$ are the light intensities along axes tilted by $\pm\pi/4$ with respect to the z axis, I_+ and I_- are the left- and right-hand circular light intensities, respectively, and I_{tot} is the total light intensity.

III. RESULTS

Light linearly polarized along z optically pumps atomic spin alignment ($\kappa = 2$) along **B**. Since the spin polarization is along **B**, the magnetic torque on the atomic spins is 0; the
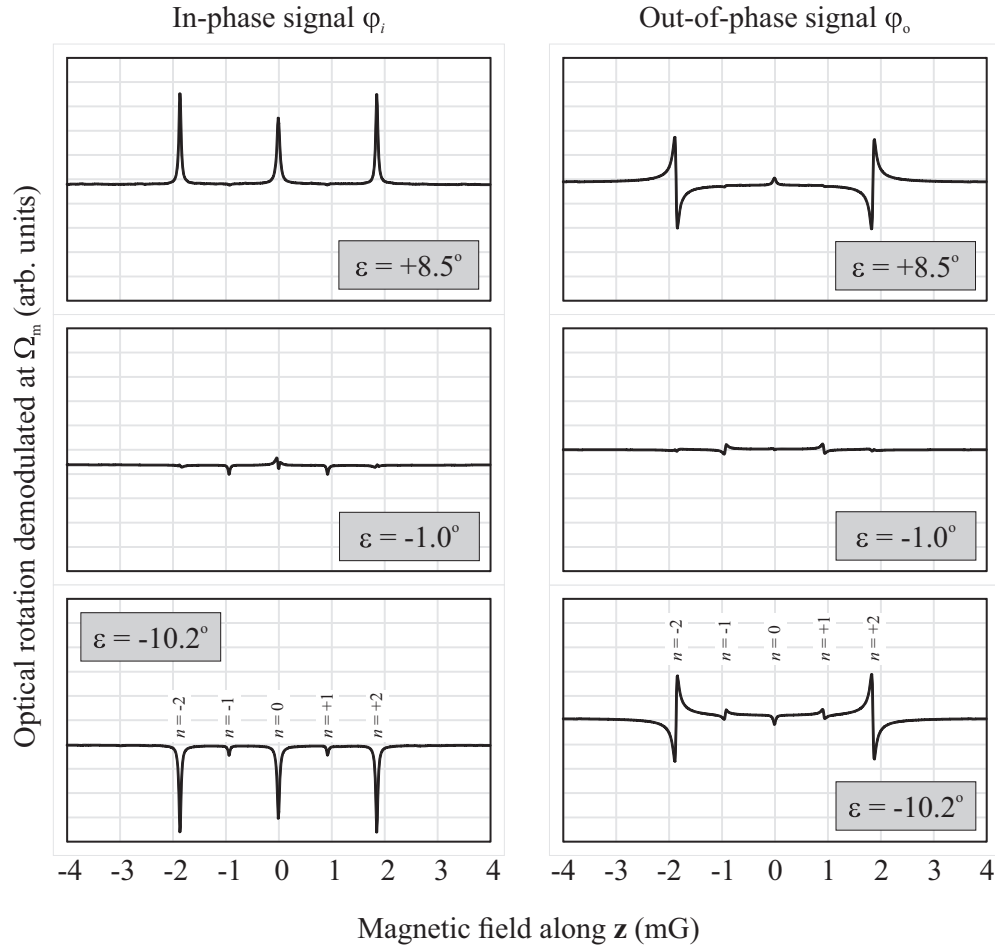
FIG. 2. Nonlinear magneto-optical rotation φ as a function of the applied magnetic field along the light polarization axis z for different values of ellipticity ε, where ε is measured in front of the vapor cell (prior to light entering the cell). The optical rotation signal is demodulated with a lock-in amplifier at the first harmonic of the laser modulation frequency Ω_m. Left: In-phase component φ_i. Right: Out-of-phase component φ_o. Light power, 500 μW; laser tuned to the high-frequency wing of the ^{85}Rb $F = 3 \to F'$ transition; modulation frequency $\Omega_m = 2\pi \times 1$ kHz; frequency-modulation amplitude $\Delta\omega = 2\pi \times 65$ MHz. Magnetic resonances occur when $\Omega_L = \Omega_m/\kappa$, where the $n = \pm 2$ resonances correspond to the $\kappa = 1$ condition and the $n = \pm 1$ resonances correspond to the $\kappa = 2$ condition. The zero-magnetic-field resonance, labeled $n = 0$, generally has contributions from all κ. The $n = \pm 1$ resonances for the $\varepsilon = -1.0°$ case, where the *in situ* ellipticity of the light is near zero, are due primarily to misalignment between the major axis of the polarization ellipse and the z axis, leading to signals arising from precession of atomic alignment [54] and alignment-to-orientation conversion [50,55]. Similar misalignment causes the appearance of $n = \pm 1$ resonances for the $\varepsilon = -10.2°$ case as well. For these data, absolute calibration of the optical rotation angles was not carried out so the vertical axes are given in arbitrary units.

spin polarization is static and does not precess. If the light is elliptically polarized, it optically pumps both alignment along z and orientation ($\kappa = 1$) along $\pm \mathbf{k}$ (depending on its helicity), where $\mathbf{k}$ is the wave vector of the light. Spins oriented along $\pm \mathbf{k}$ experience a nonzero torque from $\mathbf{B}$ and precess. If the light-atom interaction is modulated synchronously with Ω_L, macroscopic precessing orientation is generated. As the spin orientation precesses, the circular birefringence of the atomic medium is modulated, which in turn generates oscillating optical rotation. This results in EI FM NMOR resonances when $\Omega_m = \Omega_L$, the so-called $n = \pm 2$ resonances, as shown in Fig. 2. The plots on the left show the magnetic-field dependence of the amplitude of the oscillating optical rotation in phase with the modulation of the light-atom interaction, labeled φ_i, and the plots on the right show the amplitude of the out-of-phase optical rotation, labeled φ_o (see, for example,

Refs. [50,56] for more details concerning the in-phase and out-of-phase optical rotation).

The choice of geometry is important for minimization of systematic effects. In the upper plots of Fig. 2, which show the magnetic-field dependence of optical rotation for ellipticity $\varepsilon = 8.5°$, the major axis of the polarization ellipse is apparently well aligned with $\mathbf{B}$. This is evident from the fact that the amplitudes of the $n = \pm 1$ FM NMOR resonances are relatively low. On the other hand, noticeable $n = \pm 1$ resonances appear in the lower plots in Fig. 2, for $\varepsilon = -10.2°$, indicating poor alignment of the major axis of the polarization ellipse with $\mathbf{B}$. The $n = \pm 1$ FM NMOR resonances correspond to the $\kappa = 2$ resonance condition, $\Omega_L = \Omega_m/2$, which, as discussed above, is related to the atomic spin alignment. The atomic spin alignment can precess if the major axis of the polarization ellipse is tilted with respect to $\mathbf{B}$ and, in fact, can generate
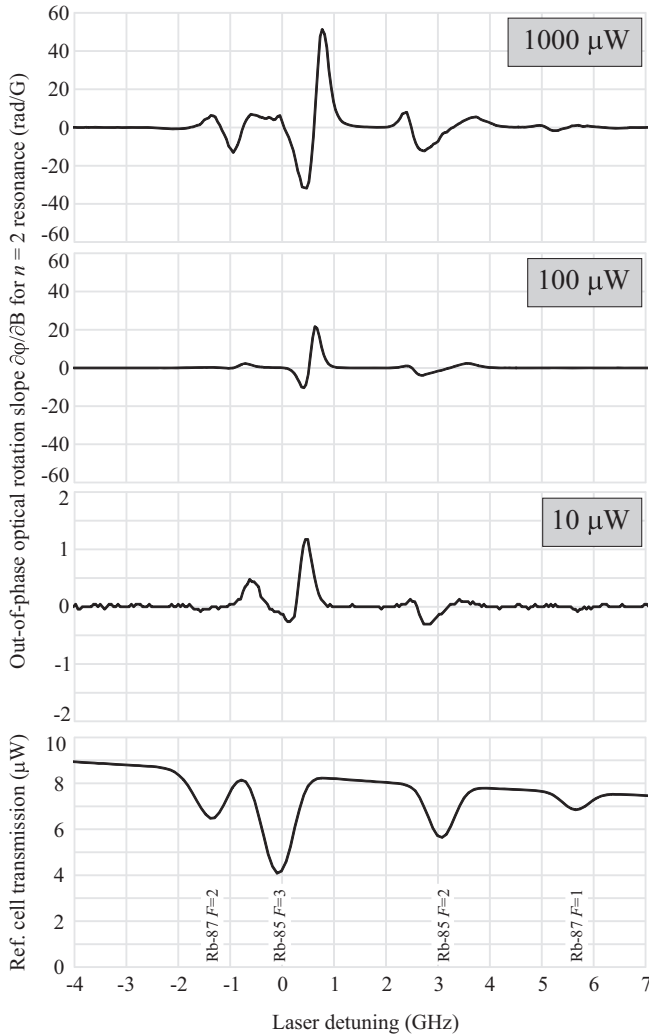
FIG. 3. The upper three plots show the slope ($\partial\varphi_o/\partial B$) of the out-of-phase component of the $n = 2$ EI FM NMOR signal as a function of the laser detuning for different incident light powers (10, 100, and 1000 μW, as indicated in the upper right corners). The lower plot shows the absorption spectrum of unmodulated light transmitted through a Rb reference cell. Light ellipticity as measured in front of the vapor cell is $\varepsilon = 8.3°$; other conditions are the same as for the data shown in Fig. 2. Note the change in the scale of the vertical axis (30×) between the plot for light power 10 μW and the plots for 100 and 1000 μW.

both $n = \pm1$ resonances and $n = \pm2$ resonances, depending on the tilt with respect to **k**, as discussed in detail in Ref. [54]. Additionally, if the optically pumped atomic alignment is tilted with respect to **B**, the phenomenon of alignment-to-orientation conversion [50,55] can occur, where tensor light shifts coupled with Zeeman shifts induce more complicated evolution of the PMs [45]. Alignment to orientation can generate $n = \pm2$ optical rotation signals that overlap with the EI FM NMOR resonances. Fortunately, the $n = \pm1$ resonances themselves can be used to align the major axis of the polarization ellipse along **B** by making adjustments until their amplitude is minimized. To achieve pure linear polarization, this suggests an iterative process where the $n = \pm1$ FM NMOR resonances are minimized to align **B** with the light polarization axis and
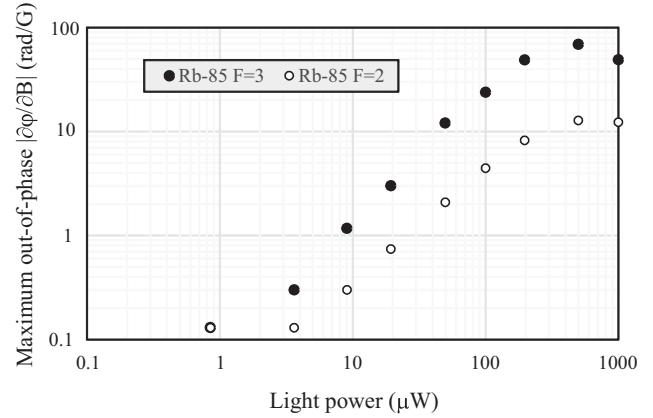

FIG. 4. The magnitude of the slope ($|\partial\varphi_o/\partial B|$) of the out-of-phase component of the $n = 2$ optical rotation signal maximized with respect to laser detuning as a function of the incident light power for the two ^{85}Rb hyperfine components. Conditions are the same as for the data shown in Fig. 3.

the $n = \pm2$ resonances are minimized to bring ε to 0. The important role of light modulation should be emphasized: for unmodulated light (as used in Ref. [26]), there is only an $n = 0$ NMOR resonance to which PMs with different κ values all contribute, making their effects difficult to discriminate experimentally.

Figure 3 shows the spectral dependence of the $n = 2$ EI FM NMOR signals for three representative light powers by plotting the slope of the out-of-phase component of the optical rotation with respect to the magnetic field, $\partial\varphi_o/\partial B$, evaluated at $\Omega_L = \Omega_m$. Studying $\partial\varphi_o/\partial B$ helps eliminate the contribution of non-B-dependent background optical rotation to the spectra, for example, that due to self-rotation of the elliptically polarized light [57]. For reference, the transmission spectrum without laser frequency modulation is displayed at the bottom in Fig. 3 and the corresponding hyperfine components are labeled. At all light powers studied, the largest $\partial\varphi_o/\partial B$ is obtained when the laser light is detuned to the high-frequency wing of the ^{85}Rb $F = 3 \rightarrow F'$ transition. Similar results have been found in past NMOR studies [34–36,50] and are attributed to the role of the bright cycling transition, $F = 3 \rightarrow F' = 4$. When the light is resonant with the $F = 3 \rightarrow F' = 4$ transition, atoms are optically pumped into a bright state that interacts more strongly with the light. Another important factor causing the EI FM NMOR signal to be maximized on the slope of a Doppler-broadened optical resonance is that the $\Omega_m = \Omega_L$ resonance condition depends on modulation of the *light-atom interaction*. If the laser is tuned to the center of a Doppler-broadened transition, the light-atom interaction is actually being modulated at $2\Omega_m$, which does not fulfill the resonance condition (see the detailed discussion of a similar situation in FM NMOR in Ref. [50]).

Figure 4 shows the detuning-maximized $|\partial\varphi_o/\partial B|$ as a function of the incident light power for the ^{85}Rb $F = 3 \rightarrow F'$ (filled circles) and ^{85}Rb $F = 2 \rightarrow F'$ (open circles) transitions. Note that the maximum $|\partial\varphi_o/\partial B|$ as a function of the light power occurs near the same power for both transitions (≈500 μW) and, also, that there is a monotonic increase up to the maximum power for both transitions. This
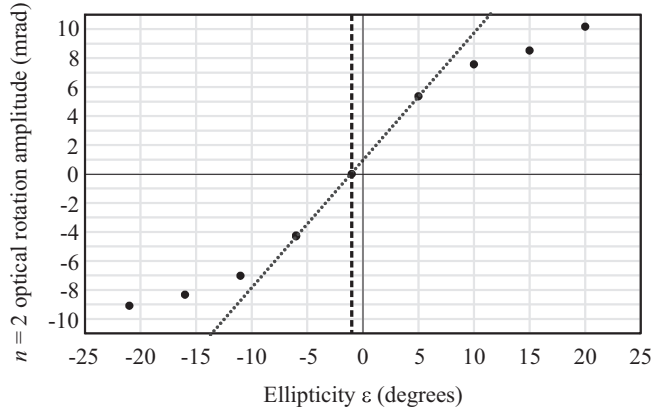
FIG. 5. The magnitude of the $n = 2$ in-phase component of the magneto-optical rotation resonance as a function of ellipticity ε, where ε is measured in front of the entrance to the vapor cell. Light power, 500 μW; other conditions the same as for the data shown in Fig. 2. The dotted gray line shows the linear slope $\partial\varphi_i/\partial\varepsilon$ in the vicinity of the zero crossing for φ_i. The thick dashed black line shows the offset of the φ_i zero crossing of the optical rotation from $\varepsilon = 0$ is a result of the birefringence of the vapor cell walls, which induces ellipticity in nominally linearly polarized light. Zeroing the $n = 2$ ellipticity-induced FM NMOR resonance can minimize the value of ε for light within the cell.

is in contrast to the situation for linearly polarized light in the Faraday geometry [50,55], where at sufficiently high light powers, alignment-to-orientation conversion becomes a dominant mechanism causing optical rotation, changing the sign of NMOR and FM NMOR effects and leading to nonmonotonic behavior of the detuning-maximized rotation. This is in agreement with the expectation that due to the chosen geometry (major axis of the light polarization ellipse along **B**), alignment-to-orientation conversion should not play any significant role in EI FM NMOR. The maximum of $|\partial\varphi_o/\partial B|$ as a function of the light power can be explained by saturation effects related to optical pumping out of the probed ground-state hyperfine level into the unprobed ground-state hyperfine level (see discussions of related saturation phenomena in Refs. [13,23,35,50], where maxima occur at similar light powers).

Figure 5 shows the magnitude of the $n = 2$ EI FM NMOR in-phase component as a function of ε for an incident light power of 500 μW. The light is tuned to the high-frequency wing of the ^{85}Rb $F = 3 \to F'$ transition where EI FM NMOR is maximized. For sufficiently small ε, we find that

$$\frac{\partial\varphi_i}{\partial\varepsilon} = 8.7 \times 10^{-4} \text{ rad/deg.} \qquad (7)$$

The standard quantum noise limit for polarimetry is

$$\delta\varphi = \frac{1}{2\sqrt{N_{\text{ph}}}}, \qquad (8)$$

where N_{ph} is the number of photons per second detected by the polarimeter. For a light power of 500 μW, Eq. (8) gives $\delta\varphi \approx 10^{-8}$ rad/$\sqrt{\text{Hz}}$. Thus we find that the projected photon
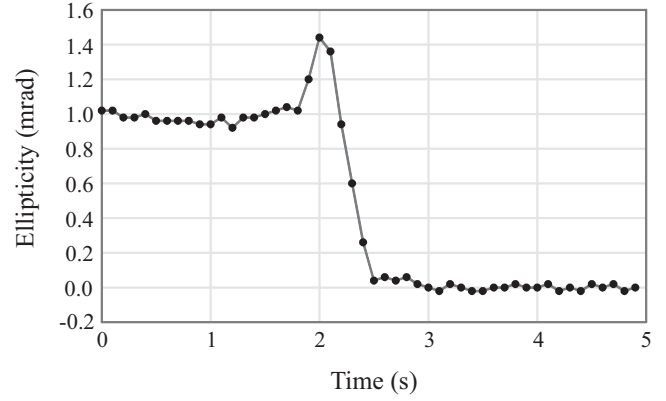

FIG. 6. Measurement of ellipticity ε using EI FM NMOR. The ellipticity is changed by hand via rotation of a linear polarizer preceding a $\lambda/4$ plate at time $t \sim 2$ s. Light power, 100 μW; other conditions the same as in Fig. 2.

shot-noise-limited sensitivity to ellipticity is

$$\delta\varepsilon = \left(\frac{\partial\varphi}{\partial\varepsilon}\right)^{-1} \delta\varphi \approx 2 \times 10^{-7} \frac{\text{rad}}{\sqrt{\text{Hz}}}. \qquad (9)$$

Shot-noise-limited polarimetry is routinely achieved in experiments using modulated light [16,21,30,31], and in our case our polarimeter is a factor of ≈ 3 above the shot-noise limit [16,50].

This can be compared to the best existing measurement of ellipticity, that described in Ref. [18], which is at the 10^{-5}-rad level but which involves the use of ultracold atoms in an optical lattice. The EI FM NMOR technique described here is technically much simpler to implement and, if one averages for only ≈ 100 s, would represent an improvement in measurement sensitivity to ε compared to Ref. [18] by roughly three orders of magnitude, illustrating the efficiency of EI FM NMOR techniques for ellipticity measurements.

One can also see the offset of the zero crossing of the EI FM NMOR amplitude from $\varepsilon = 0$, where ε was measured for the incident light prior to entering the vapor cell using the ThorLABs PAX720IR1-T polarimeter system. This indicates a systematic offset of ε from nominal zero inside the cell, presumably caused by birefringence of the cell walls. This demonstrates the usefulness of EI FM NMOR as an *in situ* light polarization measurement technique. In fact, EI FM NMOR is used to zero the ellipticity of probe light in order to minimize vector light shifts in our ongoing experiment searching for a spin-gravity coupling [16]. We anticipate that this method will be similarly useful in other precision measurements of atomic spin precession.

Figure 6 shows a measurement of ellipticity ε as determined by the calibration shown in Fig. 5, where now $\varepsilon = 0$ is taken to be the zero crossing of φ_i. For the data shown in Fig. 6, the light polarization is adjusted by hand to zero the ellipticity by rotating the linear polarizer preceding the $\lambda/4$ plate before the light enters the vapor cell (see Fig. 1). This is the final stage of an iterative process using both the $n = 1$ and the $n = 2$ EI FM NMOR resonances to align the major axis of the polarization ellipse along **B** by minimizing the $n = 1$ resonance amplitudes and zeroing the ellipticity by

minimizing the $n = 2$ resonances. The measured ellipticity, averaged over the last 2 s of data shown in Fig. 6, has an uncertainty of 3.4×10^{-6} rad, demonstrating the precision of the method. The precision of the measurement is lower than the shot-noise limit for two reasons: (i) as mentioned above, our polarimeter operates a factor of ≈ 3 away from the shot-noise limit due to technical noise, and (ii) the light power used in this measurement is 100 μW rather than 500 μW, so φ_i is a factor of ≈ 3.5 away from its maximum value.

IV. ACCURACY OF ELLIPTICITY MEASUREMENT

The accuracy with which ε can be measured is evaluated by consideration of possible systematic errors. Systematic errors due to birefringence of optical elements (such as the vapor cell walls) before and after the atomic sample are negligible since the EI FM NMOR signal is produced by the atoms themselves and has a sharp resonant character in optical frequency, modulation frequency, and magnetic field. As described above, for our geometry where the major axis of the polarization ellipse is along **B**, the symmetry of the system prevents any appearance of $n = \pm 2$ resonances occurring at $\Omega_m = \Omega_L$ unless $\varepsilon \neq 0$. Thus we conclude in principle and observe in practice (see Fig. 2) that the dominant systematic error comes from deviation from this ideal geometry: if the major axis of the polarization ellipse is rotated by an angle θ with respect to **B**, then we observe $n = \pm 2$ FM NMOR resonances even when $\varepsilon = 0$, as discussed in detail in Ref. [54]. However, as noted above, FM NMOR offers a useful tool with which to independently measure and minimize θ, namely, the $n = \pm 1$ FM NMOR resonances. Again from symmetry considerations, to first order elliptically polarized light does not affect the amplitude of the $n = \pm 1$ FM NMOR resonances since they occur at $\Omega_m = 2\Omega_L$ and are related to the $\kappa = 2$ atomic spin alignment. If the major axis of the polarization ellipse is aligned along **B**, the atomic spin alignment does not precess and thus cannot generate the $n = \pm 1$ FM NMOR resonances. Note that in this geometry, alignment-to-orientation effects are also zeroed [50,55]. By zeroing the amplitude of the $n = \pm 1$ FM NMOR resonances, the misalignment angle θ can also be zeroed and the primary systematic error can be controlled. The amplitudes of both the non-ellipticity-induced $n = \pm 2$ resonances and the $n = \pm 1$ resonances scale as θ^2 for $\theta \ll 1$. Using the techniques described in Ref. [54] we can tune

$\theta \lesssim 10^{-4}$ rad, which generates an $n = \pm 2$ FM NMOR resonance amplitude of $\approx \pm 4 \times 10^{-11}$ rad under our experimental conditions. This translates to a systematic uncertainty in ε of $\approx \pm 10^{-9}$ rad. This is far below the statistical uncertainty of the measurement shown in Fig. 6 and supports the conclusion that the measurement is statistically limited. After minimization of ε using this procedure, measurements of vector light shifts in this system are consistent with $\varepsilon \lesssim 2 \times 10^{-4}$ as discussed in Ref. [16].

V. CONCLUSIONS

In considering the application of EI FM NMOR to other systems of interest (such as cold atoms and nitrogen-vacancy centers in diamonds), we note that since our measurement is statistics limited, the sensitivity to ε scales as $1/\sqrt{NT_2}$, where N is the number of atoms (in our case $N \approx 10^{12}$) atoms. Another point to be noted is that in our experiment, because the Rb atoms are contained in an evacuated, antirelaxation-coated cell, the quantity measured is in fact the average ellipticity across the light beam, since the atoms are not spatially localized [58]. Such motional averaging is reduced in the case of cold atoms, nitrogen-vacancy centers in diamonds, and vapor cells filled with buffer gas. In these cases it should be possible to use EI FM NMOR to study the spatial profile of ε.

In conclusion, we have introduced and characterized an *in situ* method to measure and control the ellipticity of light interacting with atomic vapors: ellipticity-induced nonlinear magneto-optical rotation of frequency-modulated light (EI FM NMOR). This relatively straightforward method can be applied in experiments, for example, where precise and accurate control of vector light shifts is important.

[1] B. S. Mathur, H. Tang, and W. Happer, Phys. Rev. **171**, 11 (1968).

[2] B. R. Bulos, A. Marshall, and W. Happer, Phys. Rev. A **4**, 51 (1971).

[3] C. Cohen-Tannoudji and J. Dupont-Roc, Phys. Rev. A **5**, 968 (1972).

[4] W. Happer, Rev. Mod. Phys. **44**, 169 (1972).

[5] O. Mandel, M. Greiner, A. Widera, T. Rom, T. W. Hänsch, and I. Bloch, Phys. Rev. Lett. **91**, 010407 (2003).

[6] Y.-J. Lin, R. L. Compton, K. Jimenez-Garcia, J. V. Porto, and I. B. Spielman, Nature **462**, 628 (2009).

[7] D. M. Stamper-Kurn and M. Ueda, Rev. Mod. Phys. **85**, 1191 (2013).

[8] Y. Wang, X. Zhang, T. A. Corcovilos, A. Kumar, and D. S. Weiss, Phys. Rev. Lett. **115**, 043003 (2015).

[9] G. K. Brennen, C. M. Caves, P. S. Jessen, and I. H. Deutsch, Phys. Rev. Lett. **82**, 1060 (1999).

[10] R. Chicireanu, K. D. Nelson, S. Olmschenk, N. Lundblad, A. Derevianko, and J. V. Porto, Phys. Rev. Lett. **106**, 063002 (2011).

[11] J. A. Sherman, N. D. Lemke, N. Hinkley, M. Pizzocaro, R. W. Fox, A. D. Ludlow, and C. W. Oates, Phys. Rev. Lett. **108**, 153002 (2012).

[12] K. Jensen, V. M. Acosta, J. M. Higbie, M. P. Ledbetter, S. M. Rochester, and D. Budker, Phys. Rev. A **79**, 023406 (2009).

[13] D. Budker and D. F. Jackson Kimball, *Optical Magnetometry* (Cambridge University Press, Cambridge, UK, 2013).

[14] M. Vengalattore, J. M. Higbie, S. R. Leslie, J. Guzman, L. E. Sadler, and D. M. Stamper-Kurn, Phys. Rev. Lett. **98**, 200801 (2007).

[15] M. V. Romalis and E. N. Fortson, Phys. Rev. A **59**, 4547 (1999).

[16] D. F. Jackson Kimball, I. Lacey, J. Valdez, J. Swiatlowski, C. Rios, R. Peregrina-Ramirez, C. Montcrieffe, J. Kremer, J. Dudley, and C. Sanchez, Ann. Phys. **525**, 514 (2013).

[17] M. D. Swallows, T. H. Loftus, W. C. Griffith, B. R. Heckel, E. N. Fortson, and M. V. Romalis, Phys. Rev. A **87**, 012102 (2013).

[18] K. Zhu, N. Solmeyer, C. Tang, and D. S. Weiss, Phys. Rev. Lett. **111**, 243006 (2013).

[19] A. Kastler, Nucl. Instrum. Methods **110**, 259 (1973).

[20] A. A. Wood, L. D. Turner, and R. P. Anderson, Phys. Rev. A **94**, 052503 (2016).

[21] G. Birich, Y. V. Bogdanov, S. Kanorskii, I. Sobelman, V. Sorokin, I. Struk, and E. Yukov, J. Russ. Laser Res. **15**, 455 (1994).

[22] M. Durand, J. Morville, and D. Romanini, Phys. Rev. A **82**, 031803 (2010).

[23] D. Budker, W. Gawlik, D. F. Kimball, S. M. Rochester, V. V. Yashchuk, and A. Weis, Rev. Mod. Phys. **74**, 1153 (2002).

[24] D. Budker and M. Romalis, Nat. Phys. **3**, 227 (2007).

[25] V. V. Yashchuk, D. Budker, W. Gawlik, D. F. Kimball, Y. P. Malakyan, and S. M. Rochester, Phys. Rev. Lett. **90**, 253001 (2003).

[26] A. B. Matsko, I. Novikova, M. S. Zubairy, and G. R. Welch, Phys. Rev. A **67**, 043805 (2003).

[27] M. Auzinsh, D. Budker, D. F. Kimball, S. M. Rochester, J. E. Stalnaker, A. O. Sushkov, and V. V. Yashchuk, Phys. Rev. Lett. **93**, 173002 (2004).

[28] D. Petrosyan and Y. P. Malakyan, Phys. Rev. A **70**, 023822 (2004).

[29] N. Otterstrom, R. Pooser, and B. J. Lawrie, Opt. Lett. **39**, 6533 (2014).

[30] G. Vasilakis, J. M. Brown, T. W. Kornack, and M. V. Romalis, Phys. Rev. Lett. **103**, 261801 (2009).

[31] J. M. Brown, S. J. Smullin, T. W. Kornack, and M. V. Romalis, Phys. Rev. Lett. **105**, 151604 (2010).

[32] W. C. Griffith, M. D. Swallows, T. H. Loftus, M. V. Romalis, B. R. Heckel, and E. N. Fortson, Phys. Rev. Lett. **102**, 101601 (2009).

[33] S. Kanorsky, A. Weis, and J. Skalla, Appl. Phys. B **60**, S165 (1995).

[34] D. Budker, V. Yashchuk, and M. Zolotorev, Phys. Rev. Lett. **81**, 5788 (1998).

[35] D. Budker, D. F. Kimball, S. M. Rochester, V. V. Yashchuk, and M. Zolotorev, Phys. Rev. A **62**, 043403 (2000).

[36] D. Budker, D. F. Kimball, V. V. Yashchuk, and M. Zolotorev, Phys. Rev. A **65**, 055403 (2002).

[37] M. V. Balabas, T. Karaulanov, M. P. Ledbetter, and D. Budker, Phys. Rev. Lett. **105**, 070801 (2010).

[38] C. Chin, V. Leiber, V. Vuletić, A. J. Kerman, and S. Chu, Phys. Rev. A **63**, 033401 (2001).

[39] I. Bloch, Nature **453**, 1016 (2008).

[40] T. Kennedy, J. Colton, J. Butler, R. Linares, and P. Doering, Appl. Phys. Lett. **83**, 4190 (2003).

[41] G. Balasubramanian, P. Neumann, D. Twitchen, M. Markham, R. Kolesov, N. Mizuochi, J. Isoya, J. Achard, J. Beck, J. Tissler *et al.*, Nat. Mater. **8**, 383 (2009).

[42] W. Gawlik, L. Krzemień, S. Pustelny, D. Sangla, J. Zachorowski, M. Graf, A. Sushkov, and D. Budker, Appl. Phys. Lett. **88**, 131108 (2006).

[43] S. Pustelny, A. Wojciechowski, M. Gring, M. Kotyrba, J. Zachorowski, and W. Gawlik, J. Appl. Phys. **103**, 063108 (2008).

[44] S. Pustelny, D. F. Jackson Kimball, S. M. Rochester, V. V. Yashchuk, W. Gawlik, and D. Budker, Phys. Rev. A **73**, 023817 (2006).

[45] S. M. Rochester and D. Budker, Am. J. Phys. **69**, 450 (2001).

[46] T. Yabuzaki and T. Ogawa, J. Appl. Phys. **45**, 1342 (1974).

[47] I. Novikova, A. B. Matsko, V. L. Velichansky, M. O. Scully, and G. R. Welch, Phys. Rev. A **63**, 063802 (2001).

[48] B. Patton, E. Zhivun, D. C. Hovde, and D. Budker, Phys. Rev. Lett. **113**, 013001 (2014).

[49] A. Ben-Kish and M. V. Romalis, Phys. Rev. Lett. **105**, 193601 (2010).

[50] D. Jackson Kimball, L. R. Jacome, S. Guttikonda, E. J. Bahr, and L. F. Chan, J. Appl. Phys. **106**, 063113 (2009).

[51] S. Xu, S. M. Rochester, V. V. Yashchuk, M. H. Donaldson, and D. Budker, Rev. Sci. Instrum. **77**, 083106 (2006).

[52] D. F. Jackson Kimball, J. Dudley, Y. Li, S. Thulasi, S. Pustelny, D. Budker, and M. Zolotorev, Phys. Rev. D **94**, 082005 (2016).

[53] M. Auzinsh, D. Budker, and S. Rochester, *Optically Polarized Atoms: Understanding Light-Atom Interactions* (Oxford University Press, New York, 2010).

[54] S. Pustelny, W. Gawlik, S. M. Rochester, D. F. Jackson Kimball, V. V. Yashchuk, and D. Budker, Phys. Rev. A **74**, 063420 (2006).

[55] D. Budker, D. F. Kimball, S. M. Rochester, and V. V. Yashchuk, Phys. Rev. Lett. **85**, 2088 (2000).

[56] Y. P. Malakyan, S. M. Rochester, D. Budker, D. F. Kimball, and V. V. Yashchuk, Phys. Rev. A **69**, 013817 (2004).

[57] S. M. Rochester, D. S. Hsiung, D. Budker, R. Y. Chiao, D. F. Kimball, and V. V. Yashchuk, Phys. Rev. A **63**, 043814 (2001).

[58] E. Zhivun, A. Wickenbrock, J. Sudyka, B. Patton, S. Pustelny, and D. Budker, Opt. Express **24**, 15383 (2016).